A System-level Approach to Single-Molecule Live-Cell Fluorescence Microscopy

Oliver Harriman and Mark Christian Leake

Single-molecule fluorescence microscopy provides a window into the molecular activity of the living cell. Through genetically fusing molecules of interest with fluorescent proteins, specific biological mechanisms can be elucidated. While the approach is maturing rapidly with the application of numerous inventive optical and analytical techniques, it is still a challenge to generate adequate imaging conditions.

This article addresses the question of how an experiment can be optimally configured in order to produce the best possible data. We present development of a model of the combined instrumentation and sample that concurrently and accurately computes with the relevant quantitative information. This is used to explore the effect of parameter changes on system-level properties, such as image contrast, that are critical to achieving our experimental goals.

Introduction

The Challenge of Single-Molecule Live-Cell Fluorescence Microscopy

Single-molecule investigation has emerged over the last thirty years as a new paradigm for experimentation. Probing of individual molecules can give a depth of information that is not present in ensemble-average measures. The dynamic and static heterogeneity of molecules, manifest as differences in stable or metastable free energy states across a population of molecules, may now be accessed. A single molecule may now be observed as its free energy state changes with time. Furthermore, the energy states of numerous molecules may be differentiated simultaneously.

With rapid technological development, many single-molecule techniques have been applied in the biological sciences (Claridge, Schwartz et al. 2011). Fluorescence microscopy, empowered by highly sensitive cameras and selectively bound fluorophores, has become a core technique in the study of biomolecular activity. Work in our single-molecule biophysics research group has given some insights into the organisation and dynamics of proteins in living cells (Leake, Chandler et al. 2006; Reyes-Lamothe, Sherratt et al. 2010; Badrinarayanan, Reyes-Lamothe et al. 2012). This has been achieved primarily through the generation of strains with fluorescent protein fusion constructs, and the development and use of bespoke microscopes.

One focus is the use of Objective-lens-type Total-Internal-Reflection-Fluorescence (TIRF) microscopy to investigate the activity of electron transporter proteins in the inner membrane of *E. coli* cells (Lenn, Leake et al. 2008). The benefit of TIRF microscopy in this case is that it enables significantly higher imaging contrast due to the preferential excitation of the cell membrane over the cell cytoplasm. This reduces the contribution of fluorescence not associated with the proteins of biological interest (Figure 1).

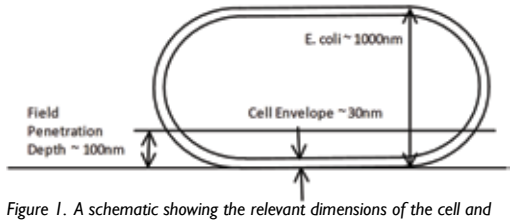

Figure 1. A schematic showing the relevant dimensions of the cell and the extent of the evanescent field.

Using multiple colours allows interesting questions to be addressed such as whether functionally linked molecules are colocalised in the cell (Figure 2).

Even with a well-suited technique, achieving intelligible data can be very challenging and a lengthy process of experimental parameter optimisation is typically necessary. Effort is made to balance several parameters in order to reach multiple system-level objectives. As a reduced example, one might want to capture the dynamics of a biological process lasting in the order of seconds in which changes in energy/conformational state might occur in the order of tens of milliseconds. One would need to find adequate laser intensities to balance high time resolution (requiring high excitation intensities

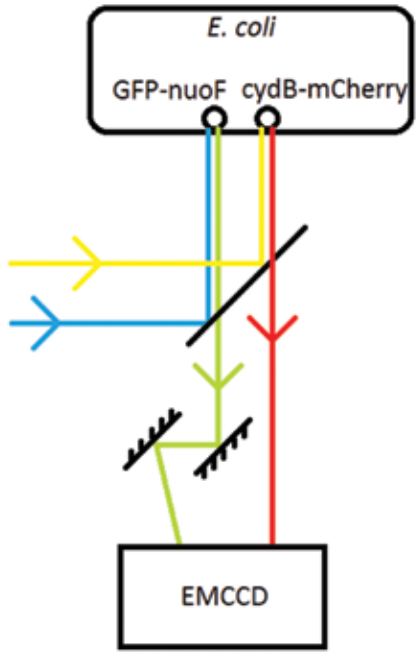

Figure 2. A simplified schematic of a two-colour experiment.

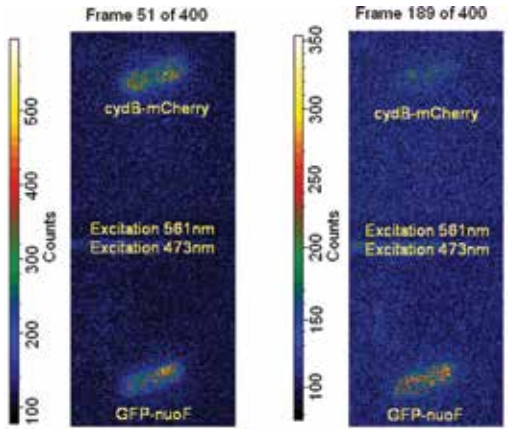

*Figure 3. False-coloured frames from a video of a fluorescently labelled **E. coli** cell. Low signal, high background and photobleaching are evident.*

for adequate signal-to-noise-ratio (SNR) with low photobleaching rate (requiring low excitation intensities in order that the video may last the entire duration of the process) (Figure 3). It is also important to consider camera settings such as the use of binning (Swift and Trinkle-Mulcahy 2012).

While it is simpler to consider a reduced model of the experimental system when changing a parameter, data quality is a function of the system as a whole. In live-cell fluorescence microscopy, many key relationships are non-linear with dependencies that are challenging to reliably envisage and qualitatively combine. Though the instrument can effectively be used as a deterministic system, the interrogation of a living cell means one must be mindful of stochasticity and history dependence.

A System-level Model-based Approach

A view was taken that our experimentation should be engaged with at the system-level. This article presents a range of efforts aimed to enhance our experiments through internally consistent computational models. These were based on what was seen to be relevant information, much of which is not typically considered systematically. Quantitative modelling was explored as a means to improve capabilities of the instrument, to enable calculation of new physical values, and to improve the performance of the experimental system (i.e. obtain higher quality data).

A review was initially carried out into the methodologies used in other fields where systems modelling and development is central. Most striking were two emerging frameworks that attempt to enable the rationalisation, practical representation and optimisation of complex systems. These were Model Based Systems Engineering (MBSE) using the SysML graphical modelling language (Bahill and Szidarovszky 2009), and Multidisciplinary Design Optimisation (MDO) (Agte, de Weck et al. 2010). Also of interest was Design of Experiments (DoE), a statistical approach to efficiently explore the parameter space of industrial experiments (Antony 2003).

Careful modelling will force one to be explicit about the assumptions and extent of knowledge of an experiment. If the modelling is clean (Martin 2008), the experimental reasoning will then be transparent and could be improved by anyone with expertise and a digital copy. If members of a research microscopy group developed a common fluency in computational modelling, one could imagine work being centred on maintenance and improvement of a model representing the shared understanding of the experimental system. This model would serve as the central artefact of hypothesis, instrument control, and analysis. Rigorous validation through real world experimentation is fundamental since computational models can be as easily misinterpreted and as flawed as mental models.

The majority of this article covers what (in MDO) is termed Design Optimisation. This involves quantitatively analysing the effect of parameter changes in a given model structure. The creation of the structure is termed 'architecture' and some interesting literature exists on effective approaches to it (Maier 2009; Mandenius and Björkman 2011). In optimising the performance of an experimental

system, architecture is generally more important to consider than the design. An example of an architectural decision was to use the TIRF scheme of microscopy to image membrane bound proteins. A review article was written to assist the key architectural decision of selecting an appropriate single-molecule technique from the diversity that now exists (Harriman and Leake 2011).

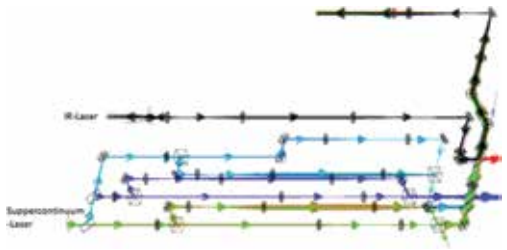

Figure 4. Illumination Architecture of bespoke microscope represented in ray tracing software.

A bespoke microscope was built to be a test-bed for the computational approaches presented here (and hence to be usable for optimised live-cell experimentation). A second goal was to develop the architecture to concurrently enable multiple imaging functionalities in order to better make use of limited resources. The illumination path of the microscope incorporates laser-tweezers with three colour channels selected from a supercontinuum laser source. Each colour channel has independently controllable S- and P-polarised beams that are either collimated or focussed at the sample with changeable expansion factors (Figure 4).

Model-instructed instrumentation schemes

This section presents a few techniques that make use of models to enable a new kind of functionality or solve a problem in a different way.

Prescriptive Polarisation-based Power Distribution

As a first example, a relatively simple optical scheme will be used to demonstrate how a model based approach may improve the capabilities of an

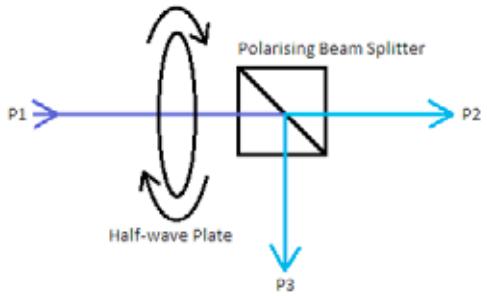

Figure 5. Rotating the half wave-plate changes the ratio of the output powers.

instrument and reduce the number of necessary components. The combination of a half-wave plate and polarizing beam splitter is commonly used to continuously attenuate a laser beam of constant power. This scheme is also used to vary the relative

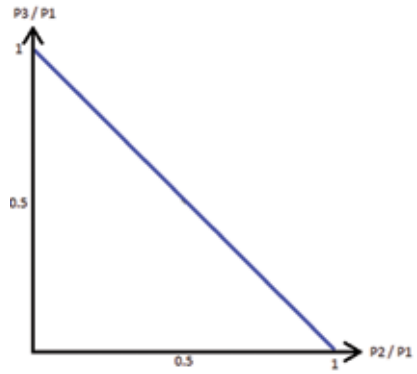

Figure 6. The blue line indicates the possible simultaneous output powers in the scheme of Figure 5.

proportions of power going into two channels (Figure 5). The sum of output powers is constrained to equal the input power (Figure 6).

For independent control of the power in each output path further components are necessary. A

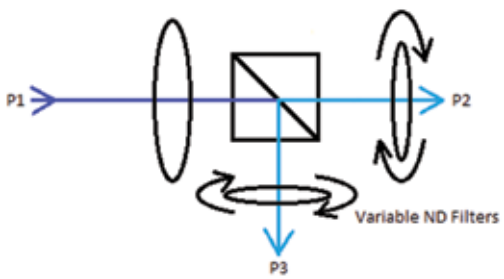

Figure 7. Independent power control is achieved with variable neutral density filters.

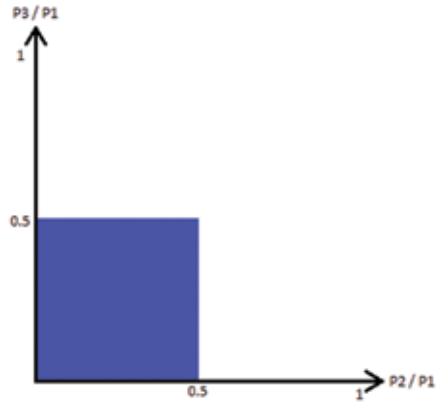

Figure 8. The possible range of powers of the scheme in Figure 7 is limited by the setting of the half-wave plate.

straightforward solution involves putting a rotating variable neutral density (ND) filter in each of the split channels (Figure 7). In practice, the half-wave plate could be set to split the beam 50:50, and then independent power control of each split channel would be achieved with the respective ND filter. This is a very pragmatic scheme, however it has limitations (Figure 8). To produce a split of 80:10, the half wave-plate would need to be rotated and then both ND filters reset.

In order to achieve independent control and the full range of power for each path, two options exist: either one could measure the power while changing the angles or the necessary angles could be calculated from the equations that describe

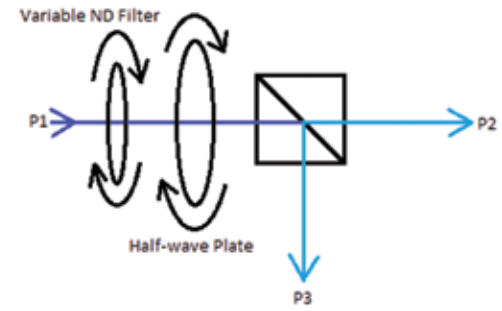

Figure 9. This scheme achieves independent control but relys on prescriptive control from a model.

transmission through the system. If one uses the second approach, a single ND filter prior to the polarising beam splitter will achieve the same function as two after (Figure 9). One simply need specify the desired powers in order to determine the necessary settings (Figure 10).

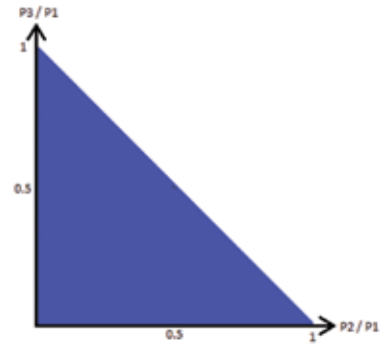

Figure 10. With the scheme in Figure 9, the maximum range of simultaneous output powers can be produced.

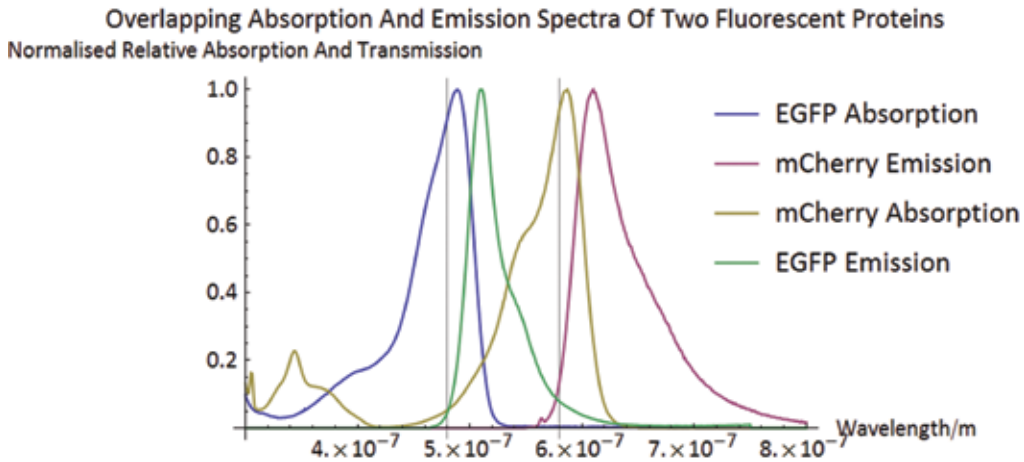

Figure 11. Spectra normalised by height for ease of comparison.

Band Selection from a Supercontinuum Spectrum

From inspecting the absorption and emission spectra of two commonly used fluorescent proteins, one can identify approximately optimal wavelengths for excitation (Figure 11). As well as for obtaining a high signal, this choice is important in reducing a number of effects including: photobleaching, phototoxicity and the artefacts known as crosstalk and bleedthrough. Using monochromatic light leaves the maximal bandwidth for collection of fluorescent emissions.

Rather than use multiple lasers for different wavelengths, one might use one supercontinuum source, giving flexibility to select arbitrary bands from the visible range. However, since the total power is spread out over the visible and IR spectra, there is potential for being power limited if using only a thin band from the spectrum. In this scenario the fluorescence emission gained from broadening the band of illumination may outweigh the emission lost from the resulting smaller band for collection of fluorescence.

With the IR component of a supercontinuum beam removed, the remaining spectral component was measured at a series of laser power settings (Figure 12). A simulation model was implemented to investigate how the selected spectral bands could be optimised computationally for different scenarios.

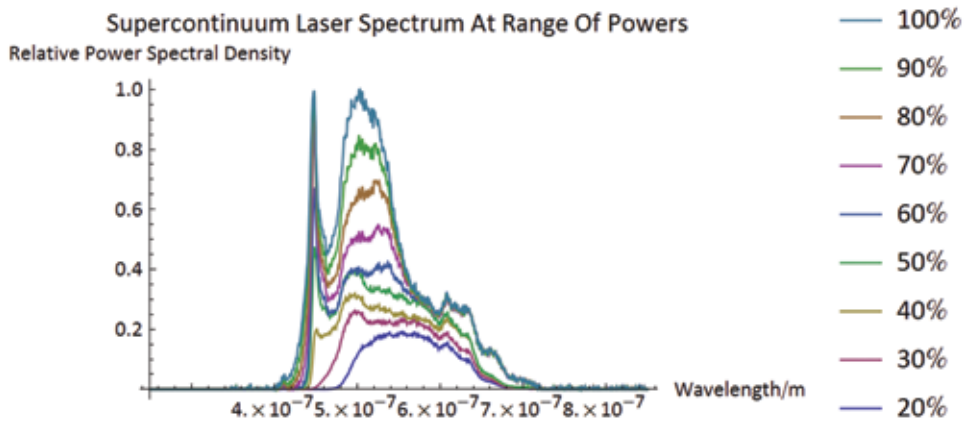

Figure 12. Supercontinuum Spectra at a series of powers.

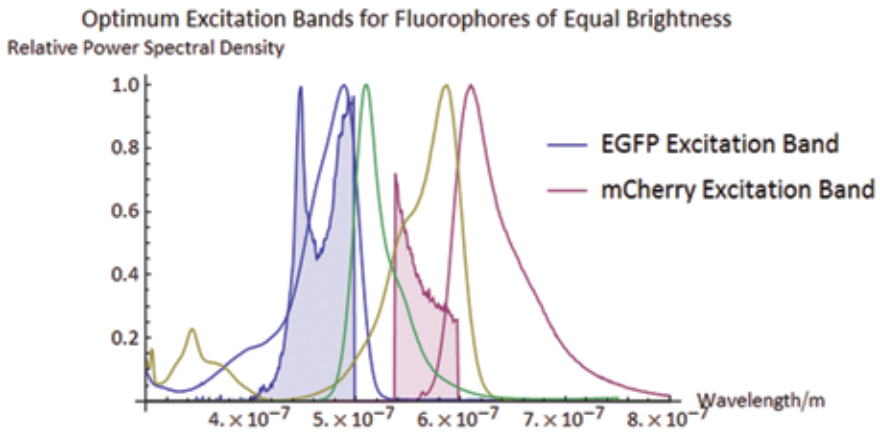

Figure 13. The optimal bands from the suprecontinuum spectrum for exciting similarly bright fluorophores.

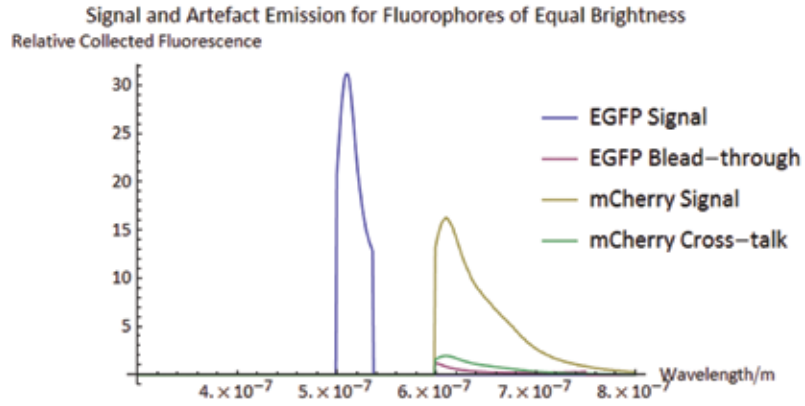

Figure 14. The fluorescent emission resulting from the illumination in Figure 13.

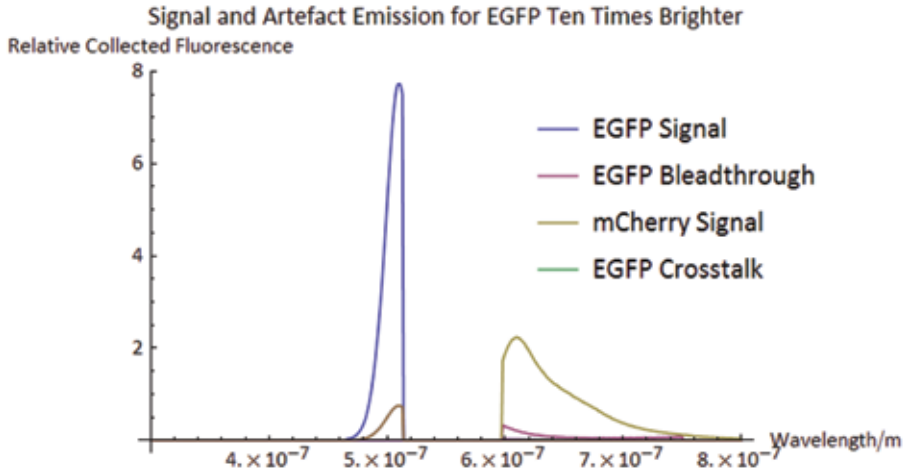

Figure 15. The optimal illumination bands can be seen to change with the relative brightness of the two fluoropohres.

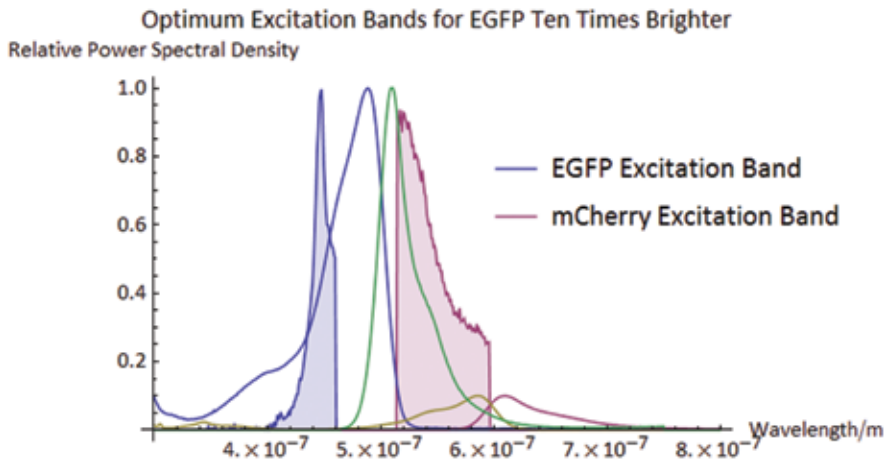

Figure 16. The fluorescent emission resulting from the illumination in Figure 15.



Figure 17. Reverse ray-tracing from desired sample illumination through lenses all on a comon axis.



Figure 18. Two steering lenses are moved by a known distance laterally to make the beam ultimately follow the axis.

The spectral selection method was based on the pattern of dichroic mirrors used in the microscope (Figure 4) where the two bands were selected by setting the cut-off wavelengths of three dichroic mirrors. To identify the cut-off wavelengths giving best performance, an objective function was evaluated at every point in the three-dimensional parameter space and the maximum value identified. The objective calculated the sum of the two emission signals (minus their respective artefact levels) and subtracted the magnitude of their differences. This led to a maximum where the signal in both bands was high.

Several scenarios were investigated. In the first case, both fluorophores were given approximately the same inherent brightness. The optimal illumination bands (Figure 13) and the resulting signal and artefacts are displayed in Figure 14.

In another case, mCherry was given a much lower inherent brightness. It can be seen that this results in a significant change in the optimal illumination bands (Figure 15) and output fluorescence (Figure 16).

Reverse Ray Tracing for Prescriptive Beam Steering

In practice, alignment is a process of trial and improvement. If it could be done prescriptively it would save time and enhance reproducibility. With the support of ray-tracing software it may be possible. The key technique is to trace rays in the reverse direction, essentially defining a desired outcome in order to determine the necessary cause.

Reverse ray-tracing was carried out to explore the necessary lens positioning to achieve a desired sample illumination. A commonly used

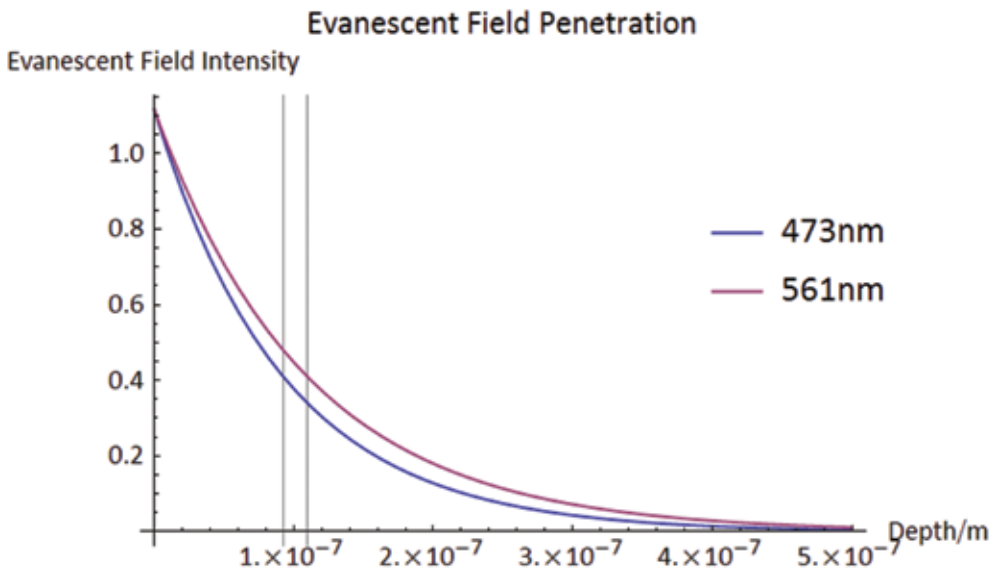

Figure 19. The field intensity against distance from the interface for two wavelengths at the same incident angle.

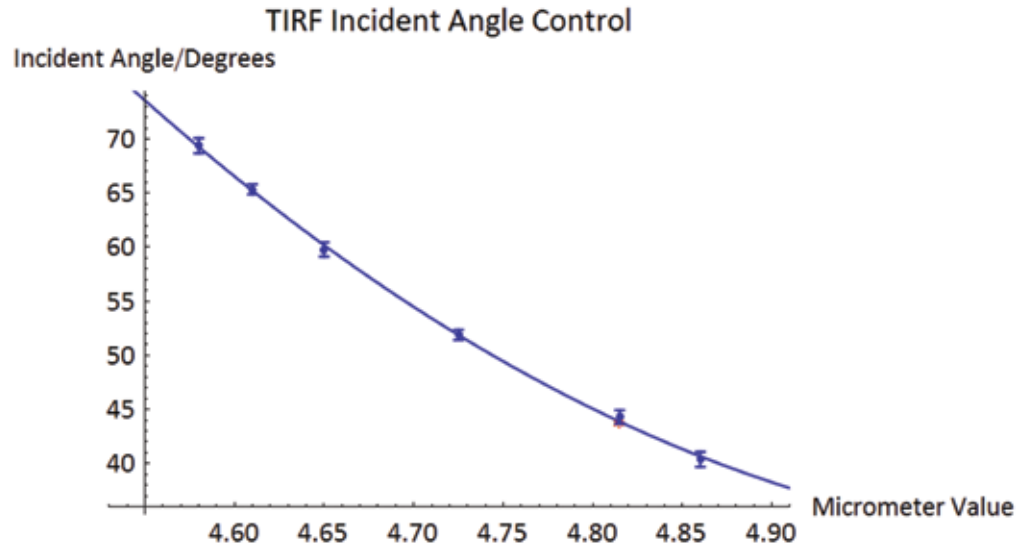

Figure 20. Example graph generated for setting the angle of incidence with a micrometre.

high NA objective lens was modelled from the patent literature. Then control lenses were added on a common axis their spacing was optimised using a programmed merit function. The desired illumination was then traced backwards through the lens system (Figure 17).

Two beam control lenses were then moved the lateral distances necessary to produce the trajectory emanating from the source in the actual instrument (Figure 18). Values of displacement could be read from the software.

The ability to do this relies on being able to specify positions of components in reality as in the model. The model was of use in analysing the sensitivity of the system with respect to the precision with which components could be positioned.

Evanescent Field Specification for High Membrane Contrast

There are subtleties to the understanding of the evanescent field. The evanescent intensity beyond the interface can be greater than the incident intensity (Axelrod, Burghardt et al. 1984). Also, the incident beam intensity will drop as incident angle increases, due to increasing eccentricity of the intersection of beam and interface. A simplified model was made to investigate how the evanescent field could be generated to maximise membrane (Figure 19).

An objective function was written to maximise the absolute value of membrane excitation and the ratio of membrane to cytoplasm excitation. Excitation was approximated by integrals of the field intensity up to and beyond the thickness of the cell envelope. An optimum angle of incidence (around 67 degrees) was found that was neither sensitive to changing the incident wavelength from 473nm to 561nm nor from changing the cell envelope thickness from 30nm to 100nm.

A technique was developed to enable prescription of this incident angle. For this, a kinematic mirror mount was modified to be actuated reproducibly with a micrometre and a device was made to measure angles incident upon the coverslip. A series of respective measurements were taken and the results automatically plotted for convenience (Figure 20).

Modelling the Whole Experimental System

So far, only subsystem models have been presented. Here, methods are presented for generation of

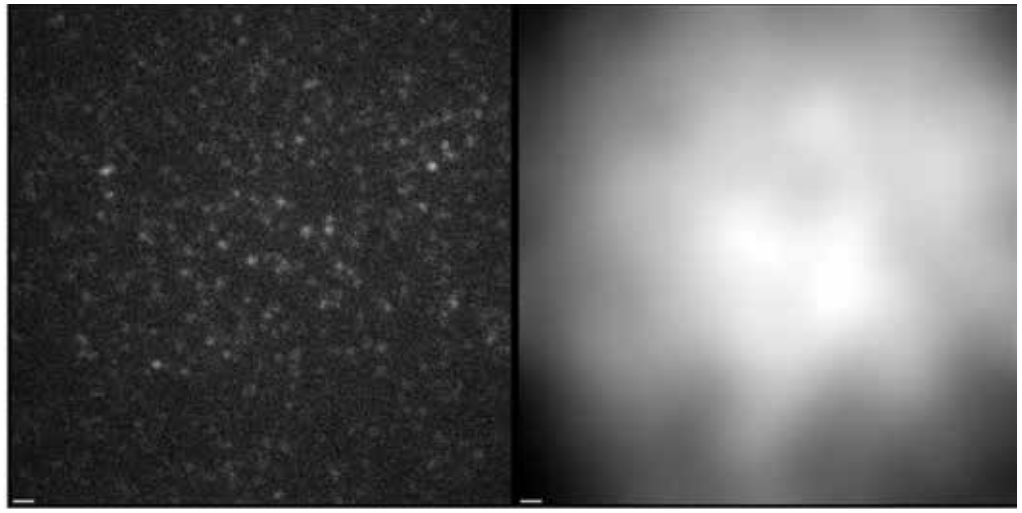

Figure 21. Images illustrative of the process of producing an illumination field intensity map. Left: TIRF illumination of randomly distributed EGFP molecules. Right: The blurred summation of five EGFP images. 1 micron scale bars.

semi-empirical models of the sample illumination and single-molecule response. The aim is the implementation of a unified model of the whole experiment.

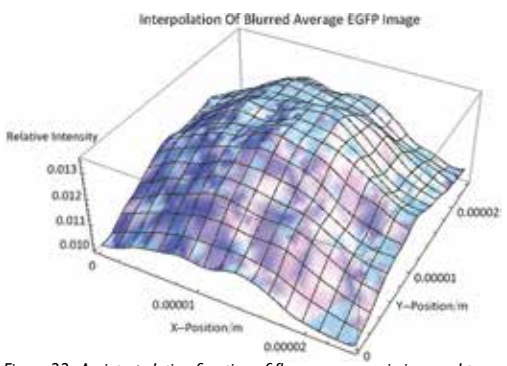

Figure 22. An interpolating function of fluorescence emission used to approximate the form of sample illumination.

With a validated whole experiment model, one need not speculate on the effect of changing a parameter. Rapid processing and efficient search algorithms can be applied to find optimal parameter settings for a given experimental goal. Sensitivity analysis, varying each parameter independently to determine the magnitude of the effect on image quality, can be used to rank parameter significance. This in turn can be used to prioritise acquisition of improved components or to better inform the process of architecting.

Three-dimensional Mapping of the Excitation Field

The intensity of fluorescence emission is used to discern a number of single-molecule characteristics. To compare fluorescence observed in different regions in an image one must know the relative illumination intensities. This is since, up to the point of saturation, the emission is approximately proportional to the excitation. Knowing the absolute intensity would enable reproducibility of experiments. A method was therefore developed to produce a three-dimensional map of the absolute illumination intensity.

The total laser beam power entering the microscope was measured and multiplied by the

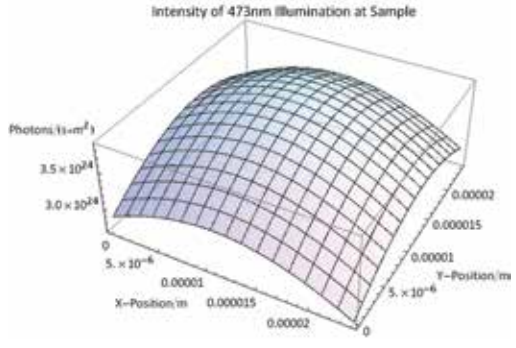

Figure 23. Absolute intensity of EGFP illumination at the focal plane.

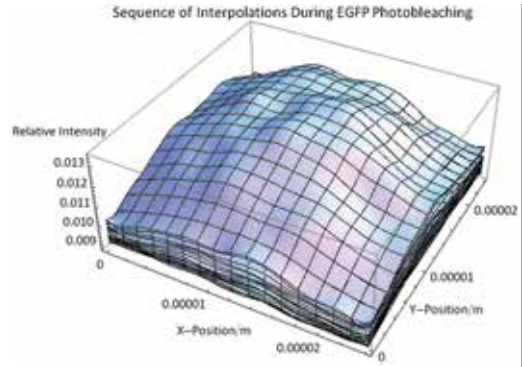

Figure 24. Frame-by-frame photobleaching illustrated by reduction in interpolated fluorescent emission.

measured transmission from the point of beam entry to the sample. This value was used as the total incident intensity in the model of evanescence previously described. The beam angle of incidence was measured and other parameters taken from the literature.

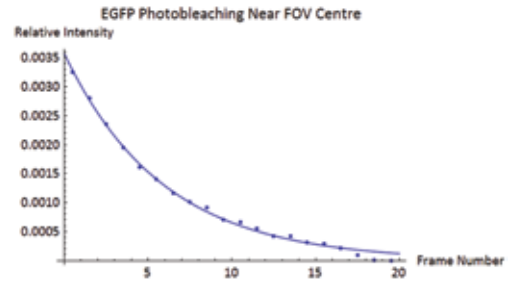

Figure 25. Photobleaching exhibited in an intensity time trace from near the centre of the image.

The beam was modelled to have a two-dimensional Gaussian profile at the interface and it was necessary to determine values for the *x* and *y* mean and standard deviation. While these parameters could have been approximated analytically, common variation in alignment dictated a need to make measurements. For this, a series of videos was taken of surface-immobilized EGFP molecules randomly distributed on a coverslip.

The first illuminated frames of each video were combined and blurred to smooth local variations in intensity. A two-dimensional interpolating function was then generated (Figure 22) and evaluated at points on a grid in the *x-y* plane.

A two-dimensional Gaussian function was fitted to the results (Figure 23) and fitting parameters extracted for generation of the field map. The integral under the whole surface (relating to the total evanescent intensity) and the *x* and *y* values of mean and standard deviation were used to parameterise the map of illumination intensity in the sample.

Modelling of Photobleaching

With an adequate SNR one often finds that photobleaching occurs too rapidly to capture enough video frames of molecular activity. For example, one may wish to track a molecule to characterise its mobility but photobleaching renders it invisible before enough trajectory information can be gained. A validated model of photobleaching could be used to explore how conditions may be altered to extend the number of frames for which SNR is adequate. In the case of two-colour imaging one may determine how to achieve maximum SNR for each colour and have both bleach after the same period of time.

A method was devised to measure the dependence of single-molecule photobleaching on illumination intensity using the same videos as for field mapping. Maps were produced for all frames in the video sequences and interpolated as before (Figure 24).

The interpolating functions were then evaluated for each frame at a grid of points in the *x-y* plane. Values were then plotted, revealing bleaching that was well described by exponential decay (Figure 25).

For each curve an exponential function was automatically fitted and the decay rate produced. These values were then plotted against their respective field intensities and a linear model was fitted. The gradient was taken as the decay constant specific to EGFP in a basic exponential decay model to describe photobleaching.

Single-molecule Brightness

Values for fluorophore brightness can be found in the literature and are calculated as the absorption

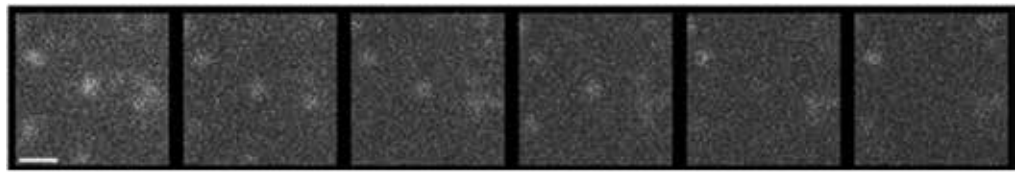

Figure 26. A sequence of micrographs (from left to right) in which a single molecule of EGFP (centre) is identified. Frames 3 and 4 were taken to exhibit a single molecule for the entirety of the exposure time and selected for analysis. 1 micron scale bar.

cross-section multiplied by the quantum yield. A method was created to compute approximate brightness values through combination of single molecule imaging (with mapped illumination intensity) and a model of the microscope emission path.

Initially sequences of images were visually inspected to identify single molecules and determine the frames for which they had been fluorescent for the entire exposure time (Figure 26). The illumination intensity of each selected fluorophore was found by its location in the field map. Each fluorophore was assumed to emit fluorescence isotropically and the proportion entering the objective lens was calculated from the numerical aperture (NA). A power meter was used to measure the attenuation of a laser beam from the sample to the camera.

The next step was to model the response of the camera to incident photons. To go from image pixel values to the number of causative incident photons, it was necessary to understand the workings of the Electron Multiplying Charge Coupled Device (EMCCD). Parameters specific to each EMCCD, the acquisition settings and the associated saturation levels and forms of noise were considered.

While noise can be described analytically, a stochastic simulation approach was taken that generated a number of parameters from probability density functions. For example, shot noise was inherent from frame to frame as a result of generating values randomly from a Poisson distribution. The simulated camera response was ultimately based on a combination of theory and data from videos taken with different conditions. The accuracy of the simulated background noise, including an optimised stray light component, was verified through comparison of histograms of real and simulated pixel values.

The point spread function was modelled with a two-dimensional Gaussian distribution and given a value of standard deviation to match the images. With all other parameters set to match the experimental, the remaining parameter to calibrate with was the value of fluorophore brightness. This was modified until a simulated image was produced that was visually comparable with the measured image (Figure 27).

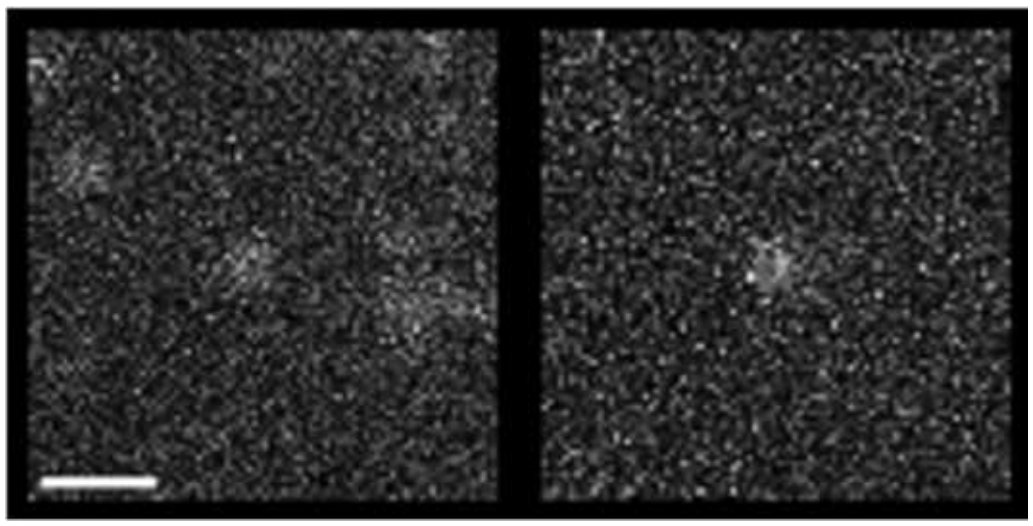

Figure 27. Left: A real image of a single EGFP molecule. Right: A simulated image calibrated to correspond to the real image. 1 micron scale bar.

Discussion

System boundaries are artificial and judgement must be exercised in the extent of what is modelled. Currently around sixty parameters are considered, many of which are general to fluorescence microscopy and some of which are specific to our instrument and samples. Features have been included that are pertinent to our experimentation such as the ability to trace bleaching of numerous fluorophores in a point spread function and the blurring associated with molecular mobility.

The model is being developed to present errors associated with simulation results. Each parameter will be generated from an appropriate distribution and the simulation will be run many times in order to build up error statistics. The code is also being restructured for faster execution and extensive optimisation searches. Significant time was invested in building the modelling framework and the necessary programming skills. This time need not be invested again by others if the model is built upon. The structure, accuracy and usability should improve with time.

The model was found to be particularly useful to a bioscientist wishing to understand fluorescence microscopy. The relevant parameters were presented in a graphical user interface and the effect of changing them could be explored with feedback from the simulated images. The code can be seen as a structured repository of all the information relevant to the experiment, including the abstract physical models that enhance understanding. Live-cell experiments have been carried out using simulation to improve data quality and will be reported in due course.

Aknowlegments

We would like to thank our colleagues in the Clarendon laboratory, in particular Dr Isabel-Llorente Garcia for the development of MATLAB image analysis software and Dr Charlotte Fournier for development of the surface-immobilized fluorescent protein assay. This work was supported by a Royal Society University Research Fellowship (M.C.L.) and EPSRC grant EP/G061009/1 (M.C.L.)

References

Agte, J., O. de Weck, et al. (2010). "MDO: assessment and direction for advancemen – an opinion of one international group." Structural and Multidisciplinary Optimization **40**(1): 17-33.

Antony, J. (2003). Design of experiments for engineers and scientists, Butterworth-Heinemann.

Axelrod, D., T. P. Burghardt, et al. (1984). "Total Internal Reflection Fluorescence." Annual Review of Biophysics and Bioengineering **13**(1): 247-268.

Badrinarayanan, A., R. Reyes-Lamothe, et al. (2012). "In Vivo Architecture and Action of Bacterial Structural Maintenance of Chromosome Proteins." Science **338**(6106): 528-531.

Bahill, A. T. and F. Szidarovszky (2009). "Comparison of dynamic system modeling methods." Syst. Engin. **12**(3): 183-200.

Claridge, S., J. Schwartz, et al. (2011). "Electrons, Photons, and Force: Quantitative Single-Molecule Measurements from Physics to Biology." ACS Nano **5**(2): 693-729.

Harriman, O. L. J. and M. C. Leake (2011). "Single molecule experimentation in biological physics: exploring the living component of soft condensed matter one molecule at a time." Journal of Physics: Condensed Matter **23**(50): 503101.

Leake, M., J. Chandler, et al. (2006). "Stoichiometry and turnover in single, functioning membrane protein complexes." Nature **443**(7109): 355-358.

Lenn, T., M. Leake, et al. (2008). "Clustering and dynamics of cytochromebd-I complexes in theEscherichia coliplasma membranein vivo." Molecular Microbiology **70**(6): 1397-1407.

Maier, M. (2009). The Art of Systems Architecting, Third Edition (Systems Engineering), CRC Press.

Mandenius, C.-F. and M. Björkman (2011). Biomechatronic Design in Biotechnology: A Methodology for Development of Biotechnological Products, Wiley.

Martin, R. (2008). Clean Code: A Handbook of Agile Software Craftsmanship, Prentice Hall PTR.

Reyes-Lamothe, R., D. Sherratt, et al. (2010). "Stoichiometry and Architecture of Active DNA Replication Machinery in Escherichia coli." Science **328**(5977): 498-501.

Swift, S. and L. Trinkle-Mulcahy (2012). "To bin or not to bin." Infocus Magazine(26): 4.

Oliver Harriman (o.harriman1@physics.ox.ac.uk), Clarendon Laboratory, Parks Road, Oxford OX1 3PU.

Oliver is a D.Phil/Ph.D student in the Single-Molecule Cellular Biophysics research group of Professor Mark Leake.

Professor Mark C. Leake (mark.leake@york.ac.uk), Anniversary Chair of Biological Physics, Depts of Physics and Biology, University of York, YO10 5DD, UK.

Mark has recently relocated his research activities to York University where he now heads the new Biological Physics Group (http://single-molecule-biophysics.org) as its Chair.







EMAG 2013

Electron Microscopy and Analysis Group Conference 2013

3–6 September 2013
University of York, York, UK

Organised by the IOP Electron Microscopy and Analysis Group

Electron microscopy is currently in an exciting period of development, with new advances in instrumentation allowing unprecedented insights into the structure, chemistry and dynamics of the nanoworld. This is having a huge impact in many fields, including materials, nanoscale devices, 2D nanostructures, bioscience and catalysis, to name just a few. This conference will focus on the latest techniques and instrumentation developments in electron microscopy, together with its applications in a variety of fields.

Conference highlights

- High profile plenary speakers
  - Prof. Ahmed Zewail (Nobel Prize in Chemistry 1999, CalTech)
  - Prof. Archie Howie (University of Cambridge)
  - Prof. Pratibha Gai (University of York)
- Special symposium in honour of Prof. Archie Howie
- Refereed proceedings
- Pre-conference short courses on advanced topics in electron microscopy (Monday 2 and Tuesday 3 September)

Exhibition

An exhibition of scientific instruments, equipment and techniques will be held alongside EMAG 2013. Visitors are welcome to browse the exhibition free of charge, please e-mail **conferences@iop.org** to register your interest.

Programme topics

Technique developments and their applications:

- The Archie Howie symposium on *in situ* microscopy
- Advances in electron microscope imaging
- Spectroscopy and analysis
- Developments in STEM
- Modelling and quantification of electron-microscope data

Applications of electron microscopy to specific areas:

- Nanomaterials
- Structural materials
- Functional materials
- Biomaterials and hard-soft matter interfaces in biomedical and environmental science

Key dates

Early registration deadline:	2 August 2013
Registration deadline:	28 August 2013

www.emag-iop.org

IOP Institute of Physics